

Electronic and optical properties of Mn impurities in ultra-thin ZnO nanowires: insights from density-functional theory

Andreia Luisa da Rosa

*Instituto de Física, Universidade Federal de Goiás,
Campus Samambaia, 74690-900 Goiânia, Goiás, Brazil and
Bremen Center for Computational Materials Science,
University of Bremen, Am Fallturm 1, 28195 Bremen, Germany*

Leticia Lira Tacca

*Instituto de Física, Universidade Federal de Goiás,
Campus Samambaia, 74690-900 Goiânia, Goiás, Brazil*

Erika Nascimento Lima

Universidade Federal de Mato Grosso, Campus Rondonópolis, 78005-050 Rondonópolis, Mato Grosso, Brazil

Thomas Frauenheim

*Bremen Center for Computational Materials Science,
University of Bremen, Am Fallturm 1, 28195 Bremen, Germany*

In this work we have employed density-functional theory with hybrid functionals to investigate the atomic and electronic structure of bare and hydrogenated Mn doped ZnO nanowires with small diameter. We determine changes in magnetic and electronic structure of Mn-doped ZnO nanowires due to surface effects, such as hydrogen adsorption on the surface, presence of oxygen vacancies and dangling bonds. In the absence of passivation on the nanowire surface, the manganese atoms segregate to the surface, whereas under hydrogen adsorption the incorporation of Mn is energetically more favourable at inner sites. The presence of additional oxygen vacancies does not produce significant changes in magnetic moments, although it produce significant changes in charge localization.

INTRODUCTION

Controlled incorporation of magnetic impurities in a semiconductor provides a means to manipulate magnetic and electronic interactions. Among transition metal ions, Mn has received long-standing interest as a dopant in semiconductors because of its large spin magnetic moment and therefore applications in spintronics[1]. ZnO (zinc oxide) is a wide band gap semiconductor which can be synthesized in several nanostructured forms. Indeed ferromagnetism due to Mn impurities above room temperature has been reported by several authors [2–7], although it has also been assigned to the formation of inclusions or secondary phases [8], while other investigations suggested a paramagnetic behavior [9–12].

Mn incorporation in ZnO nanostructures has also drawn attention [13–16]. The pioneer work by Nair *et al.*[17] reported ferromagnetism in diluted Mn-doped ZnO nanowires at temperatures up to 400 K and attributed it to an interplay between Mn doping and native point defects. More recently it has been assigned to the formation of magnetic polarons [13]. Nanowire based field-effect transistor demonstrated the presence of ferromagnetism above room temperature, suggesting that quantum confinements improves the Curie temperature [15]. Theoretical calculation suggested that Mn incorporation can be achieved, but the interaction between Mn atoms leads to an anti-ferromagnetic or paramagnetic behavior [14, 18, 19]. More recently, the interest in Mn-doped ZnO has risen due to possible applications in quantum information [20, 21]. It has been shown that inserting Mn in ZnO nanocrystals with small diameters with passivated surfaces leads a very efficient source of spin decoherence [22].

Despite all the efforts, some aspects of Mn incorporation in ZnO nanostructures remain unclear. Due to the large surface/volume ratio, effects of surface passivation by impurities or ligands can be crucial for successful doping, as discussed in Refs. [23, 24]. In this work, we address Mn insertion in ultra-thin ZnO nanowires using density functional theory [25] and hybrid-density functionals[26]. Such wires serve as ideal systems to investigate quantum confinement, since their diameter is approximately 1 nm, less than the ZnO bulk exciton Bohr radius of 2.34 nm[27]. We determine changes in magnetic and electronic structure of Mn-doped ZnO nanowires due to surface effects, such as hydrogen adsorption on the surface, presence of oxygen vacancies and dangling bonds.

We show that the impurity prefers to sit at bulk positions when the surface is adsorbed by hydrogen. On the other hand, bare wires suffer from self-purification problems leading to segregation of the dopant of Mn towards surface sites. Furthermore we find that Mn atoms in ZnO create additional states in the nanowire band gap. However, for bare wires, these states strongly hybridize with the surface states. On the other hand hydrogenated wires passivate surface dangling bonds, which appear to be beneficial for Mn incorporation. Finally we suggest that oxygen vacancies do not introduce significant changes in the overall magnetic properties. However, depending on the vacancy location, the overlap between Mn states and surface states are affected by such defects.

METHODOLOGY

Density-functional theory (DFT) [28] and the projected augmented wave (PAW) method, as implemented in the Vienna Ab initio Simulation Package (VASP) [29], has been used to investigate Mn incorporation in ultra-thin ZnO nanowires. In order to model Mn impurities in ZnO we built up an isolated, infinite wire along the [0001] direction containing 48 ZnO-units and a vacuum region of 15 Å. This gives a Mn concentration of 2.1%. To ensure convergence of structural, electronic and magnetic properties, a cutoff of 400 eV was used for the wave function expansion in plane waves. Atomic forces on all atoms were converged up to 0.001 eV/Å. Brillouin zone integration of the charge density has been done with a $(1 \times 1 \times 4)$ \mathbf{k} -point sampling. The relaxation of the nanowires was done using the PBE [30] functional. One of the key aspects in the identification of dopant states is the proper description of the band gap of the host material. While the PBE functional is very reliable to describe atomic properties, the same has limitations to describe electronic structure and optical properties in semiconductors [31, 32]. Recently the use of modern exchange-correlation functionals in density-functional theory has shown to yield band gap values close to experiment [33–35]. We have recently shown that the use of hybrid functionals can reproduce the ZnO band gap and provide correct location of energy levels of $3d$ and $4f$ in ZnO.[36–39]. Hybrid functionals are approximations to the exchange-correlation energy functional in density-functional theory that incorporate a certain amount of exact exchange from the Hartree-Fock term. The PBE0 functional [40] mixes the PBE exchange energy with the 25% of Hartree-Fock exchange energy treating the correlation at PBE level. On the other hand the HSE [26] exchange-correlation functional uses an error function screened Coulomb potential to calculate the exchange energy. This functional mix 25% of Hartree-Fock exchange in the DFT exchange energy while treating the correlation part at DFT level solely. We have used 36%, as it is found to reproduce the experimental gap of ZnO, as shown in Refs. [34, 36, 41, 42].

RESULTS AND DISCUSSIONS

The electronic band gaps for ZnO bulk in the wurtzite structure, bare and hydrogenated wires are 3.6, 4.0 and 3.6 eV, respectively. The value for ZnO bulk is slightly larger than the experimental value of 3.4 eV [41]. In bare wires, surface states appear below the bottom of conduction band due to Zn dangling bonds (around 0.5 eV) and at the top of the valence band due to O dangling bonds, reducing the band gap (not shown). The adsorption of hydrogenated wires suppresses the surface states and therefore produces a band gap close to the bulk value [43–45].

Doping of ZnO bulk with Mn splits the Mn-3*d* states into majority *e* and minority *t*₂ states, with manganese assuming a high-spin configuration (*S*=5/2). Projected local magnetic moments on Mn atoms are 5.0 μ_B . Mn in ZnO bulk produces states around 0.5 eV above the valence band maximum with a strong hybridization as shown in Fig. 3 (b).

The wire geometries we have investigated are shown in Figs. 2. A single Mn atoms is incorporated at surface (A), subsurface (B) and inner sites (C). A single Mn occupying a substitutional Zn site in the middle of the wire does not produce strong distortion in the ZnO wire lattice. For Mn sitting at subsurface/surface sites little relaxation is seen as well, as the covalent radius is similar to Zn. The Mn-O bond lengths remain very close to the values in pure ZnO, ranging from 1.8-2.1 Å in bare wires and from 2.0-2.2 Å in hydrogenated wires.

Incorporation of a single Mn impurity leads to site-dependent formation energies, as shown in Table I. For bare wires, the preferred position is the surface position A. The small volume of the nanostructure and surface effects leads to defect migration towards the surface, as it has been discussed [23, 24, 36, 46, 47]. On the other hand by passivating the nanowire surfaces with hydrogen, Mn have a lower formation energy than when it is incorporated in the bulk position C. The energy difference between bulk and surface position is 0.51 eV for bare wires and 1.35 eV for hydrogenated wires. Total magnetic moments are not sensitive neither to site position nor to passivation, although a small hybridization is found with nearest-neighbor oxygen atoms.

The total and projected density-of-states (PDOS) for Mn doped wires are shown in Figs. 3. We discuss only the energetically most stable structures for both bare and hydrogenated wires. In Fig. 3(a) we show the results for a Mn at surface site A in ZnO bare wire. The impurity produces states in the ZnO band gap located at 0.8 and 2.0 eV above the valence band maximum (VBM). This leads to a decreasing in the ZnO band gap, as it has been observed in photoluminescence experiments [48, 49]. In all cases the minority spin states lie deep inside the ZnO CBM.

The perfect ZnO (10 $\bar{1}$ 0 surface consists of pairs of ZnO units. In bulk ZnO, the atoms are fourfold coordinated, but at the surface they are three-fold coordinated exposing Zn and O dangling bonds. When the surface is hydrogenated, as a result of reaction with hydrogen molecules or water, the most stable situation is a full coverage. The stability of these structures has been discussed in Refs. [45, 50]. In fully hydrogenated wires, Mn states are located inside the valence band (VB) as it can be seen from Figs. 3 (b). Additionally, majority spin states *e* lie 1 eV above ZnO VBM and therefore hybridize with the O-2*p* states.

Whether the optical transitions involving the intragap states are allowed needs to be verified. Therefore we have calculated the dielectric function of the most stable structures, i. e., Mn at an a surface site in bare wires and Mn at an inner site in hydrogenated wires. Fig. 4 shows the imaginary part ϵ_2 of the dielectric function for the electromagnetic field propagation perpendicular ϵ_{\perp} and parallel ϵ_{basal} to the wire growth direction. The ϵ_{\perp} component shown in Fig. 4 (a) for the bare wire has an onset of 2 eV for absorption corresponding to the Mn state located in the band gap shown in 3 (c). This means that these states are optically active.

On the other hand ϵ_{\perp} in hydrogenated wires shown in Fig. 4 (b) has its absorption onset located at 3.6 eV, which is the electronic band gap of the bare ZnO wire. This means that these states are not optically active. In both cases the ϵ_{basal} component is larger. Usually ZnO nanowires grow along the [0001] direction with the non-polar surfaces exposed as facets. As we have recently shown in Ref. [51] that the incidence of the external electromagnetic field along the non-polar direction could be better for excitation response. This is again confirmed in the present work. In order to establish a correlation with experimental observations, we should mention that recently UV-vis experiments found that doping ZnO with Mn causes band gap narrowing [52]. Our results show that this corresponds to for both bare and hydrogenated wires, although with different values. ZnO has been reported to have several intrinsic defects with low formation energies, oxygen and zinc vacancies among them [35, 53–55]. In nanostructures, we have shown that O vacancies in ZnO nanowires might be present and have low diffusion barrier towards surface sites in comparison to the opposite path [47]. This kind of defect can affect the adsorption of molecules and incorporation of dopants [56, 57]. With this in mind, we have include the presence of an oxygen vacancy in the Mn placed at inner sites of ZNO nanowires. We have considered two situations: a vacancy placed close to the Mn and at a vacancy at a surface site. This is motivated by photoluminescence studies which confirmed the formation of oxygen vacancies in Mn doped ZnO nanostructures [58]. We find that the presence of a vacancy in Mn doped bare wires is more stable for a vacancy sitting at a surface site C by 1.00 eV. This is in agreement with our previous calculations where we predicted that oxygen vacancies should migrate to surface sites in bare wires [47]. Interestingly enough, the magnetic moment of these systems is not affected by the vacancy. Perhaps a more realistic picture should be an ionized vacancy

which is out of the scope of this paper.

In order to provide further insight on how the charge distribution in these wires we have calculated the band decomposed charge density. Charge localization is affected by the vacancy, but it is due to surface dangling bonds. In Figs. 5 we show the band decomposed charge density for Mn placed at the C site of a bare ZnO nanowires in the absence Figs. 5(a) and (b) and in the presence 5(c) and (d) of an oxygen vacancy at the surface of the wire. The charge is shown at the Γ point for the highest occupied state (a) and (c) and for the lowest unoccupied state (b) and (d). In the absence of defects, the charge is localized around the Mn atom for both the highest occupied and lowest unoccupied states. In the presence of an oxygen vacancy, the highest occupied state is more localized at the surface for the highest occupied state. This charge localization has also been found for ZnO non-polar surfaces [46, 59]. The lowest unoccupied states now have contributions from surface sites. We can conclude that there is a stronger charge separation when a vacancy is at a surface site. This effect appears to be more important for charge separation than the surface dangling bonds. This could be beneficial for photocatalytic processes, since it is expected that enhanced charge separation leads to longer lifetimes in photocatalytic devices [60].

I. CONCLUSIONS

We have investigated ZnO nanowires doped with Mn using hybrid density functionals. We show that the impurity prefers to sit at bulk positions when the surface is adsorbed by hydrogen. On the other hand, bare wires suffer from self-purification problems leading to segregation of the dopant of Mn towards surface sites. As metal oxide semiconductor photocatalysts are promising for fuel generation from water splitting and carbon dioxide reduction, several strategies have been employed to use nanostructured ZnO as photocatalyst. In this work we find that Mn atoms in ZnO create states in the oxide nanostructure. However, for bare wires, these states strongly hybridize with the surface states stemming from the surface sites and oxygen vacancies.

ACKNOWLEDGEMENTS

We are thankful for the financial support from the Brazilian agencies CNPq and FAPEG. A.L.R and T.F. would like to thank also German Science Foundation (DFG) under the program FO R1616.

-
- [1] T. Dietl, H. Ohno, F. Matsukura, J. Cibert, and D. Ferrand, *Science* **287**, 1019 (2000).
 - [2] P. Sharma *et al.*, *Nature Materials* **2**, 673 (2003).
 - [3] N. Theodoropoulou *et al.*, **300**, 407 (2006).
 - [4] N. S. Norberg *et al.*, *J. Am. Chem. Soc.* **126**, 9387 (2004).
 - [5] H. J. Blythe, R. M. Ibrahim, G. A. Gehring, J. R. Neal, and A. M. Fox, *J. Magn. Mag. Materials* **283**, 117 (2004).
 - [6] K. R. Kittilstved, D. A. Schwartz, A. C. Tuan, S. M. Heald, S. A. Chambers, and D. R. Gamelin, *Phys. Rev. Lett.* **128**, 3910 (2006).
 - [7] M. H. F. Sluiter, Y. Kawazoe, P. Sharma, A. Inoue, A. R. Raju, C. Rout, and U. V. Waghmare, *Phys. Rev. Lett.* **94**, 187204 (2005).
 - [8] M. A. Garcia, M. L. Ruiz-Gonzalez, A. Quesada, J. L. Costa-Kramer, J. F. Fernandez, S. J. Khatib, A. Wennberg, A. C. Caballero, M. S. Martin-Gonzalez, M. Villegas, F. Briones, J. M. Gonzales-Calbet, and A. Hernando, *Phys. Rev. Lett.* **94**, 217206 (2005).
 - [9] C. N. R. Rao and F. L. Deepak, *J. Mater. Chem.* **15**, 573 (2005).
 - [10] S.-J. Han *et al.*, *Appl. Phys. Lett.* **83**, 920 (2003).
 - [11] G. Lawes *et al.*, (2004), <http://arXiv:cond-mat/0403196>.
 - [12] S. Kolesnik, B. Dabrowski, and J. Mais, *J. Appl. Phys.* **95**, 2582 (2004).
 - [13] K. R. Sapkota, W. Chen, F. S. Maloney, U. Poudyal, and W. Wang, *Sci. Rep.* **3**, 35036 (2016).
 - [14] W. Li, G. Wang, C. Chen, J. Liao, and Z. Li, *Nanomaterials* **7**, 20 (2017).
 - [15] L.-T. Chang, C.-Y. Wang, J. Tang, T. Nie, W. Jiang, C.-P. Chu, S. Arafin, L. He, M. Afsal, L.-J. Chen, and K. L. Wang, *Nano Lett.* **14**, 1823 (2014).
 - [16] V. Strelchuk, O. Kolomys, S. Rarata, P. Lytvyn, O. Khyzhun, C. O. Chey, O. Nur, and M. Willander, *Nanoscale Research Letters* **12**, 351 (2017).
 - [17] U. Philipose, S. V. Nair, S. Trudel, C. F. Souza, S. Aouba, R. H. Hill, and H. E. Ruda, *Appl. Phys. Lett.* **88**, 263101 (2006).
 - [18] H. Shi and Y. Duan, *J. Appl. Phys.* **103**, 073903 (2008).
 - [19] A. L. Rosa and R. Ahuja, *J. Phys.: Condens. Matter* **19**, 386232 (2007).

- [20] F. Moro, L. Turyanska, J. Wilman, A. J. Fielding, M. W. Fay, J. Granwehr, and A. Patane, *Sci. Rep.* **5**, 10855 (2015).
- [21] R. E. George, J. P. Edwards, and A. Ardavan, *Phys. Rev. Lett.* **110**, 027601 (2013).
- [22] K. Benzid, A. Chetoui, M. Maamache, P. Turek, and J. Tribollet, *Europ. Phys. Journal* **104**, 47005 (2013).
- [23] S. C. Erwin, L. Zu, M. I. Haftel, A. L. Efros, T. A. Kennedy, and D. J. Norris, *Nature* **436**, 91 (2005).
- [24] A. L. Schoenhalz and G. M. Dalpian, *Phys. Chem. Chem. Phys.* **15**, 15863 (2013).
- [25] P. Hohenberg and W. Kohn, *Phys. Rev.* **136**, B864 (1964).
- [26] J. Heyd, G. E. Scuseria, and M. Ernzerhof, *J. Chem. Phys.* **118**, 8207 (2003).
- [27] Y. Gu, I. L. Kuskovsky, M. Yin, S. O'Brien, and G. F. Neumar, *Appl. Phys. Lett.* **85**, 3833 (2004).
- [28] W. Kohn and L. J. Sham, *Phys. Rev.* **140**, A1133 (1965).
- [29] G. Kresse and D. Joubert, *Phys. Rev. B* **59**, 1758 (1999).
- [30] J. P. Perdew, K. Burke, and M. Ernzerhof, *Phys. Rev. Lett.* **77**, 3865 (1996).
- [31] J. c. v. Klimeš, M. Kaltak, and G. Kresse, *Phys. Rev. B* **90**, 075125 (2014).
- [32] G. Onida, L. Reining, and A. Rubio, *Rev. Mod. Phys.* **601**, 2002 (2002).
- [33] J. Paier, M. Marsman, and G. Kresse, *Phys. Rev. B* **78**, 121201 (2008).
- [34] S. Lany and A. Zunger, *Phys. Rev. B* **81**, 113201 (2010).
- [35] S. J. Clark, J. Robertson, S. Lany, and A. Zunger, *Phys. Rev. B* **81**, 115311 (2010).
- [36] L. L. Tacca, A. L. da Rosa, E. N. Lima, and T. Frauenheim, *phys. stat. sol. (b)* (2018), <https://doi.org/10.1002/pssb.201800421>.
- [37] S. Geburt, M. Lorke, A. L. da Rosa, T. Frauenheim, R. Rder, T. Voss, U. Kaiser, W. Heimbrod, and C. Ronning, *Nano Letters* **14**, 4523 (2014).
- [38] M. Lorke, T. Frauenheim, and A. L. da Rosa, *Phys. Rev. B* **93**, 115132 (2016).
- [39] A. Dominguez, M. Lorke, A. L. Schoenhalz, A. L. Rosa, and T. Frauenheim, *J. Appl. Phys.* **115**, 203720 (2017).
- [40] C. Adamo and V. Barone, *J. Chem. Phys.* **110**, 6158 (1999).
- [41] W. M. Haynes, ed., "Crc handbook of chemistry and physics: A ready-reference book of chemical and physical data," (CRC Press, Boca Raton, 2016) 97th ed.
- [42] A. Janotti and C. G. V. de Walle, *Rep. Prog. Phys.* **72**, 126501 (2009).
- [43] H. Xu, A. L. Rosa, T. Frauenheim, R. Q. Zhang, and S. T. Lee, *Appl. Phys. Lett.* **91**, 031914 (2007).
- [44] W. Fan, H. Xu, A. L. Rosa, T. Frauenheim, and R. Q. Zhang, *Phys. Rev. B* **76**, 073302 (2007).
- [45] H. Xu, W. Fan, A. L. Rosa, R. Q. Zhang, and T. Frauenheim, *Phys. Rev. B* **79**, 073402 (2009).
- [46] H. Xu, A. L. Rosa, T. Frauenheim, and R. Q. Zhang, *phys. stat. sol. (b)* **247**, 2195 (2010).
- [47] B. Deng, A. L. da Rosa, T. Frauenheim, J. P. Xiao, X. Q. Shi, R. Q. Zhang, and M. A. V. Hove, *Nanoscale* **6**, 11886 (2014).
- [48] M. Samadi, M. Zirak, A. Naseri, E. Khorashadizade, and A. Z. Moshfegh, *Thin Solid Films* **605**, 2 (2016).
- [49] N. Kamarulzaman, M. F. Kasim, and R. Rusdi, *Nanoscale Research Letters* **10**, 346.
- [50] B. Meyer and D. Marx, *Phys. Rev. B* **67**, 035403 (2003).
- [51] D. Franke, M. Lorke, T. Frauenheim, and A. L. Rosa, *J. Phys. Chem. C* 10.1021/acs.jpcc.8b08412.
- [52] S. A. Ahmed, *Results in Physics* **7**, 604 (2017).
- [53] A. Janotti and C. Van de Walle, *Phys. Rev. B* **76**, 165202 (2007).
- [54] P. Erhart, A. Klein, and K. Albe, *Phys. Rev. B* **72**, 085213 (2005).
- [55] S. Lany, H. Raebiger, and A. Zunger, *Phys. Rev. B* **77**, 241201 (2008).
- [56] R. T. da Silva, A. Mesquita, A. O. de Zevallos, T. Chiamonte, X. Gratsens, V. A. Chitta, J. M. Morbe, G. Rahman, V. M. Garcia-Suarez, A. C. Doriguetto, M. I. B. Bernardi, and H. B. de Carvalho, *PCCP* **20**, 20257 (2017).
- [57] N. H. Moreira, A. L. da Rosa, and T. Frauenheim, *Appl. Phys. Lett.* **94**, 193109 (2009).
- [58] J. Panda, I. Sasmal, and T. K. Nath, *AIP Advances*, 6 (2016).
- [59] F. D. Angelis and L. Armelao, *Phys. Chem. Chem. Phys.* **13**, 467 (2011).
- [60] F. Opoku, K. K. Govender, C. G. C. E. van Sittert, and P. P. Govender, **41**, 8140 (2017).

TABLE I. Total and atom projected magnetic moments μ_{tot} (in μ_B). Relative formation energies E_f (in eV) of neutral Mn impurities in ZnO calculated with HSE.

site	bare				hydrogenated			
	μ_{tot}	μ_{Mn}	$\sum \mu_{\text{O}}$	E_f	μ_{tot}	μ_{Mn}	$\sum \mu_{\text{O}}$	E_f
inner	5.0	4.3	0.09	1.35	5.0	4.5	0.12	0.00
sub	5.0	4.4	0.12	0.13	5.0	4.5	0.11	0.50
surf	5.0	4.4	0.10	0.00	5.0	4.5	0.07	0.51

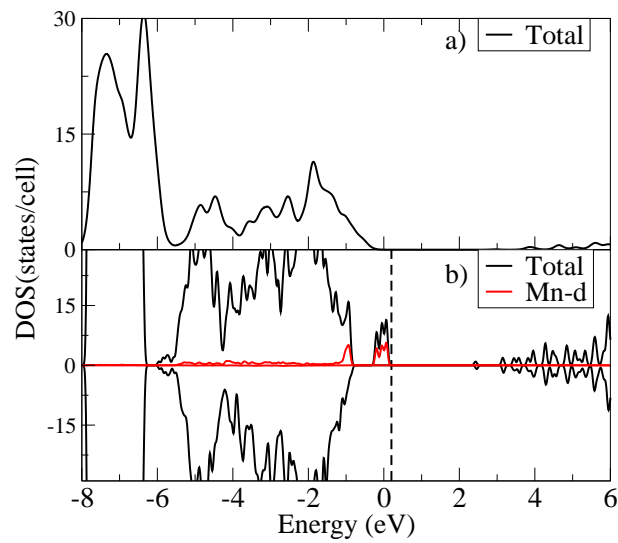


FIG. 1. Density of states of a) pure ZnO bulk and b) Mn doped ZnO bulk with a Mn concentration of 2.7%. The dashed line represents the Fermi level.

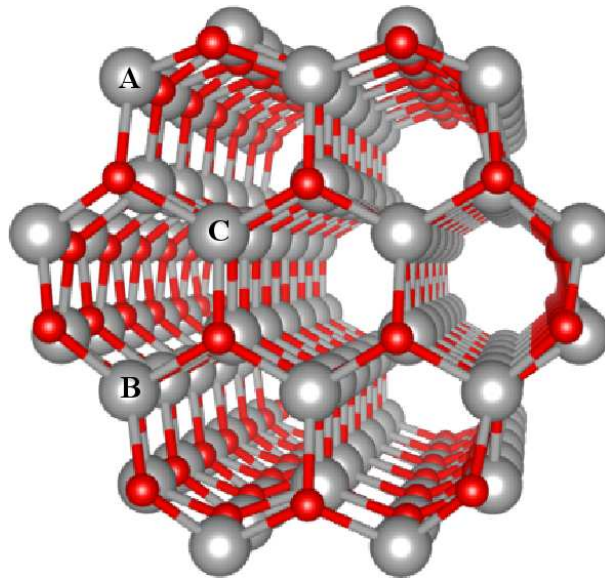


FIG. 2. Atomic configurations for Mn_{Zn} in bare ZnO nanowires. The surface A, subsurface B and inners C sites for Mn substitutional at Zn sites are indicated.

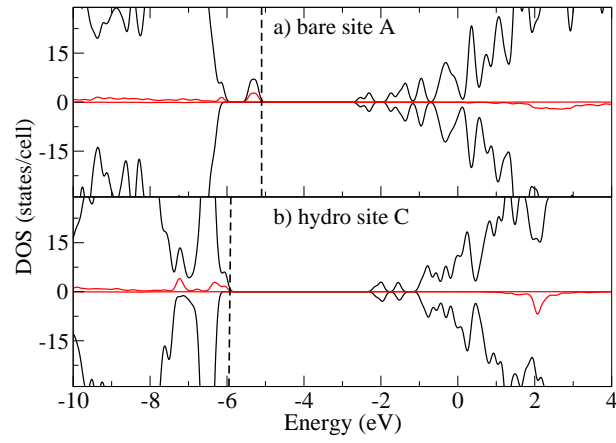


FIG. 3. Density of states of (a) Mn at surface A position in ZnO bare wires and (b) at inner C position in hydrogenated wires with HSE. The Fermi level (dashed line) is set to the highest occupied state.

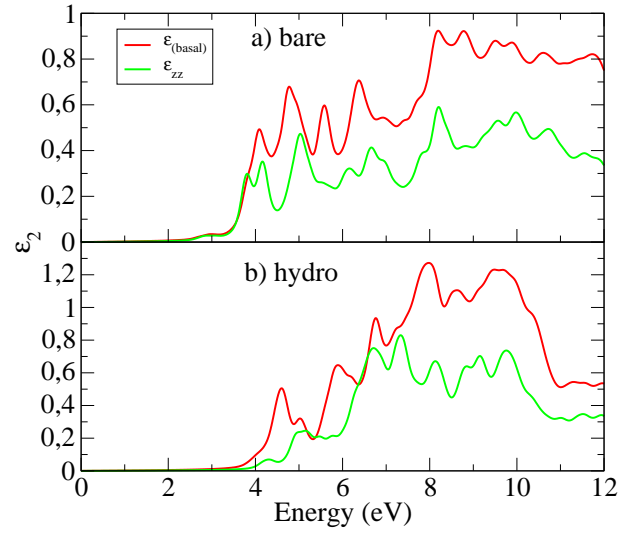


FIG. 4. Imaginary part of the dielectric function of Mn doped ZnO nanowires: a) Mn at surface site in bare wires and b) Mn at inner site in hydrogenated wires. ϵ_{zz} and (b) for ϵ_{basal} are the field propagation along the wire growth direction and along the basal plane.

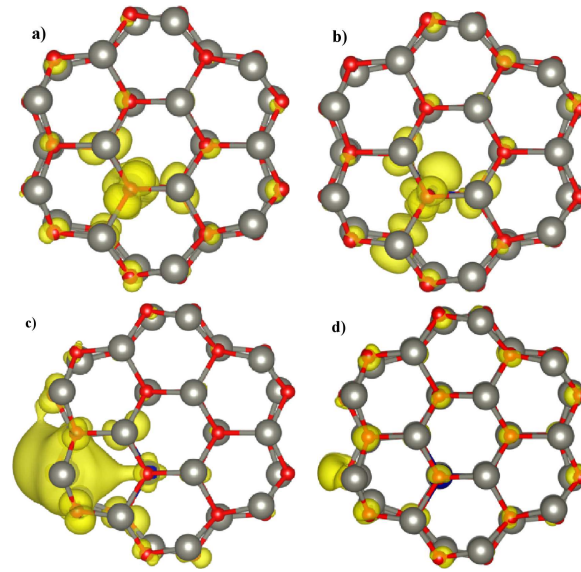


FIG. 5. Band decomposed charge density for Mn doped ZnO bare nanowires: (a) and (b) in the absence and (c) and (d) in the presence of an oxygen vacancy. The Mn atom is at the inner site C and the oxygen vacancy at the surface of the wire. The charge is shown at the Γ point for the highest occupied state (a) and (c) and for the lowest unoccupied state (b) and (d). Isosurface value is $0.0003 e \text{ \AA}^3$.